Journal of Air Pollution and Health (Summer 2019); 4(3): 171-186

Original Article

Available online at http://japh.tums.ac.ir

Sensitivity of mesoscale dust simulation to WRF_Chem boundary layer scheme (Case study: March 14th 2012)

Elham Mobarak Hassan[1,*], Parvin Ghafarian[2], Faranak Bahrami[3], Mahnaz Karim Khani[3], Morteza Sabori[4]

[1] Department of Environment, Ahvaz Branch, Islamic Azad University, Ahvaz, Iran

[2] Department of Atmospheric Science, Iranian National Institute for Oceanography and Atmospheric Science, Tehran, Iran

[3] Atmospheric Science and Meteorological Research Center, Tehran, Iran

[4] Department of Earth Science, Science and Research Branch, Islamic Azad University, Tehran, Iran

ARTICLE INFORMATION

Article Chronology:
Received 03 July 2019
Revised 23 August 2019
Accepted 01 September 2019
Published 29 September 2019

Keywords:

Mesoscale dust; WRF_Chem model; Boundary layer scheme (PBL); PM_{10}; 10-m wind speed

CORRESPONDING AUTHOR:

mobarak_e@yahoo.com
Tel: (+98 61) 33348365
Fax: (+98 61) 33348365

ABSTRACT:

Introduction: Recently, local dust events increased in Khuzestan province. Therefore, knowledge on its properties can have a crucial role in future prediction and planning.

Materials and methods: This study investigated the effect of different boundary layer schemes for dust simulation by WRF_Chem model on March 14th 2012 in Khuzestan province. To validate the model, observation data such as horizontal visibility, 10-m wind speed and PM_{10} were provided.

Results: The results indicated that the MYN scheme has the highest correlation between model outputs and observation for 10-m wind speed, PM_{10} and horizontal visibility. Due to the highest correlation of the 10 m wind speed, horizontal visibility, PM_{10} respectively with 0.83, -0.76 and 0.76 values and the highest consistency with the day-night variation of PM_{10}, MYN scheme can be selected as the most suitable scheme. At the second level, UW scheme seems to be an appropriate option. In MYN and UW schemes, the maximum wind speed in 925 hPa level was estimated 24 m/s at 03 UTC, March 14th which caused an increase in the 10 m wind speed at 06 and 09UTC. Therefore, the dust emitted from the surface to the air. Although the results of MYJ scheme showed proper correlation and temporal variation with observed, but as it determined PM_{10} concentration with high difference, it can't be considered as a suitable scheme for simulation dust concentration.

Conclusion: Although the PM_{10} concentration obtained by WRF_Chem showed difference with the observation for all the selected boundary layer schemes, MYN scheme gives the most appropriate result.

Introduction

Numerous factors are effective in the emission, vertical and horizontal transfer and dust concentration of mesoscale dust events. Increase of the arid and low-water lands provide condition for the formation of this type of dust. Inside the Iran country, unsustainable development projects in the region mainly dam construction and water transfer from one watershed to another, over consumption of the water for Sugar Cane Development and improper irrigation methods have resulted in severe decline in debit of the rivers

Please cite this article as: Mobarak Hassan E, Ghafarian P, Bahrami F, Karim Khani M, Sabori M. Sensitivity of mesoscale dust simulation to WRF_Chem boundary layer scheme (Case study: March 14th 2012). Journal of Air Pollution and Health. 2019; 4(3): 171-186.

ending to Khuzestan plain including Karoon, Dez and Karkheh. Evaluations have shown up to 9% increase in arid lands area [1]. Over consumption of upstream countries (especially Turkey) also decreased the water of Tigris and Euphrates and dried the wetlands, which led to drying of alluvial plains of Khuzestan and its wetlands. In recent years, dryness of the region land and increase of arid regions have enhanced the frequency of mesoscale dust events in this province. Knowledge on the mechanism and features of this type of dust event can play a crucial role in its prediction and planning to reduce the effect of it.

Mesoscale processes and convective activities as well as the height of planetary boundary layers have significant impact on the daily variations and vertical and horizontal transfer of dust [2]. In daytime that the land gets warm, vertical temperature profile has lower stability and the turbulence may increase which may enhance the height of the planetary boundary layer. In such condition, dust particles will move toward the higher altitudes of the atmosphere. Most of the dust and pollutant particles will remain in the boundary layer of the atmosphere. However, sometimes, some of them may enter the higher levels and the free atmosphere and be transferred to farther distances (from the land surface [3-5].

The height of planetary boundary layer (PBL) can be affected by various mechanisms among which surface features can be mentioned [6]. Surface fluxes provide the boundary condition in the lower parts of the atmosphere for vertical transfer of the physical parameters and the eddy fluxes within the PBL, which will alter the height of the PBL and change its features [7].

Increase of turbulence in daytime will enhance the surface wind speed, which has a significant impact on the dust emission. If the wind speed exceeds a threshold in a region with poor vegetation and arid soil, the conditions are provided for dust emission and dust particles will be entered into the atmosphere [8-11].

Although the threshold of wind speed in different areas is depended on the surface conditions of the soil, in most cases the wind velocity has been determined more than 6-7 m/s for the formation of dust event in the area [1, 12-15].

3D atmospheric models are important tools for understanding the meteorological parameters and their impacts on air quality models. Estimated correctly and accurate simulation of meteorological process and prediction of wind in the boundary layer are of crucial importance in simulation of chemical samples in the atmosphere, industrial activities, agriculture, air pollution and air quality management [16-23].

Atmospheric boundary layer schemes and land-surface models (LSMs) are two major parts in parameterization of the 3D atmospheric models. These two processes have close interaction with each other, are effective in wind simulation, turbulence, and hence air quality in lower levels of the atmosphere, region identification and dust or pollution transfer [20, 24-26].

Various boundary layer schemes use different assumptions for mass, humidity and energy transfer, so vertical mixing ability in lower levels of the atmosphere and absorbing the air from above layers are different and hence the height of boundary layers would be different in them [27]. These can affect the dust characteristics. Therefore, determining and recognizing the best boundary layer height in simulating weather parameters and air pollution in a particular region or in a particular situation is very important. In this study, the impacts of various WRF_Chem PBL schemes on the properties of mesoscale dust and wind speed of Khuzestan province are addressed. For this purpose, dust events on March 13 and

14 2012 were selected and simulated using different WRF_Chem boundary layer schemes. The features of the boundary layers schemes will be discussed in next sections; the data used WRF_Chem as well as its configuration is the topic of the next following section. In the findings section, the model outputs (10 m wind speed, PM_{10} concentration, PBL height and vertical distribution of the dust in the atmosphere) were analyzed and compared with the observations. The best scheme was then introduced in terms of mesoscale dust event estimation.

Planetary Boundary layer schemes in WRF_Chem model

PBL schemes are classified in two groups: local and non-local. Local schemes assume that the turbulence fluxes only depend to local values and gradients of the atmosphere variables [28]. This group uses the static stability condition in which the large eddies are under the influences of the stability with small vertical growth; therefore, the mixing will be limited in the boundary layer and its height will have a small growth. In real atmosphere and under convection condition however, large-scale eddies will transfer the heat from the ground to the higher levels of the atmosphere (without considering the maximum local stability) and vertical mixing will occur throughout the boundary layer depth [29, 30]. Eddies will penetrate to the top of the mixed layer therewith the free air attract into the PBL and reinforce it. Therefore, local schemes are poor in simulating the depth of the boundary layer, particularly during the day and in convective conditions, local schemes are limited and less credible [31].

Non-local schemes are the second group in which the flux at each point is calculated by analyzing the vertical profile of the entire mixed layer. In this method, the impact of turbulence is diffused throughout the PBL and resulted in increase of it's depth.

Generally, vertical transfer is conducted by small eddies in local schemes and large eddies in non-local. Therefore, non-local schemes estimate the boundary layers deeper compared to the local ones [32]. Therefore, non-local schemes are more accurate than the local ones [30]. In WRF_Chem model, the local schemes are UM, CAM, QNSE, TEMF, BouLac, MYNN and MYJ while YSU, GFS, MRF and ACM are the non-local schemes. Comparison of the PBL height by different schemes has been addressed in some studies. PBL schemes determined the vertical profile of the fluxes under well-mixed condition in daytime and in night stable boundary layer; they can also simulate the distribution of surface fluxes including latent and sensible heat as well as momentum transfer through turbulence not only in PBL but also throughout the atmosphere column [28].

As surface flux and turbulence govern during daytime and the condition was stable during the night, different schemes did not show similar behavior in various hours of day and night and they are sensitive to the hour. Some of research suggested that the PBL height estimated by MYJ is lower than the one obtained by YSU and non-local schemes of ACM2 and YSU estimated deeper PBL with less bias [33, 34]

Non-local schemes such as YSU and ACM2 showed more consistency with the observations compared to the others; for instance temperature and humidity had lower bias during daytime mixing [27, 35, 36]. These schemes showed lower accuracy during night [36, 37].

In some other researches, application of MYJ resulted in less bias [35].The results obtained by the local scheme of MYN were closest to observations [36]. The consistency with the observations was higher in morning hours compared to the observational data.

WRF_Chem boundary layer schemes and air pollution

Numerous studies have addressed the effect of PBL and LSM on chemistry of the atmosphere and air pollution as well as the dust events [22, 33, 38-42].

YSU scheme is widely used in chemical and atmospheric simulations [37]. This scheme is capable of realistic simulation of vertical structure of the chemical and meteorological variables of the atmosphere during day hours. For night hours, it however shows higher differences (larger bias) [24, 25].

Ozone simulation in Spain showed the lowest bias when simulated by ACM2 scheme. In case of nitrogen dioxide, the best bias was obtained when YSU was employed [36].

The impact of MYJ and YSU schemes on simulation of air pollution gases showed that the PBL height estimation by MYJ was 20-40% lower than that estimated by YUS. It also estimated higher concentrations for CO_2 and $PM_{2.5}$ compared to YSU [27, 22, 43].

As PM includes complex combination of solid and liquid particles as well as organic and mineral dust and secondary inorganic aerosols, PM_{10} concentration can be used for investigating the dust concentration. WRF_Chem model exhibited the worst results in terms of PM simulation and almost none of its schemes can simulate PM well [36]. In some points and under some conditions, the model results were not suitable and applicable [44]. Estimated PM_{10} concentration was higher than the observed values and at peak of dust, it was 70-140% higher [44]. Temporal variation of PM_{10} showed good consistency with the observations [44]. Another study however reported a good consistency of PM_{10} concentration with the observations [45].

None of the studies has considered the simulation error due to the changes in primary assumption of each scheme. The difference in the results was only considered and the best scheme was selected based on that. In addition to the difference of PBL schemes and their sensitivity to day/night hours, surface schemes are another factor in error of the simulations. This study neglected this factor.

Materials and methods

The observation data including horizontal visibility and current phenomenon were provided from the Iran meteorological organization. In meteorological reports, 07 code stands for the dust event formed in the station while code 06 represents the dust formed from outside of the station. Regarding the 07 code and the value of horizontal visibility, the dust event on March 13 and 14 2012 was selected as the mesoscale dust event.

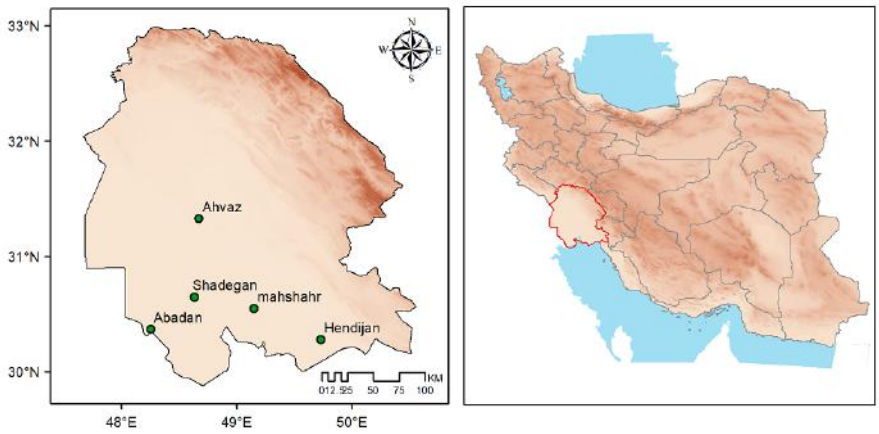

Fig. 1. The position of the stations that have reported dust with 07 code on March 14, 2012

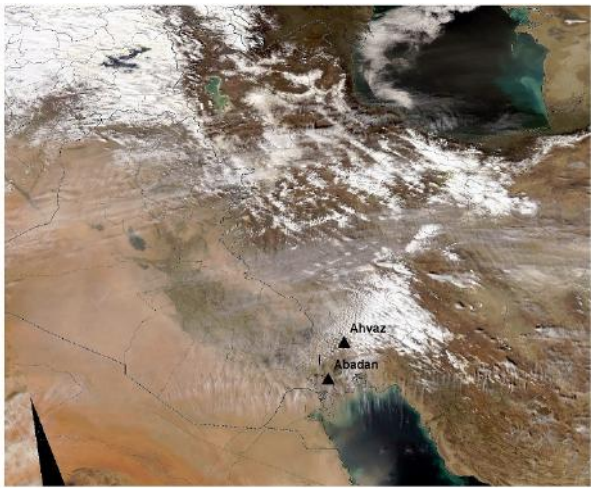

Fig. 2. The MODIS satellite image on March 14, 2012 and the location of Ahvaz and Abadan stations.

MODIS satellite image on March 14th clearly showed dust in southwest of Iran and southeast of Iraq. The presence of thick clouds on south-western Iran makes it difficult to detect dust.

In the first section, the mean sea level pressure, geopotential height at 500 hPa and wind field of 925 hPa were provided and analyzed from ERA_Interim reanalysis data (hereafter ERA_I) in spatial and temporal resolutions of 0.75 and 6 h. also these data were used as initial conditions for WRF_Chem model.

Weather Research and Forecasting/ Chemistry model (WRF_Chem) V. 3.9.1, which is a combination of Weather Research and Forecasting and atmospheric chemistry module models were used for simulating the dust events. The model was implemented in a grid with horizontal resolution of 21 km with 103, 94 and 38 points along x, y and z-axes, respectively. Table 1 lists the configuration of the applied scheme.

Table 1. The configuration of WRF_Chem model

Parameterization	Option	Planetary boundary layer	Surface layer scheme
Dust emission	GOCART	Yonsei university scheme (YSU)	MM5 similarity
Microphysics	Lin	Mellor-Yamada Nakasishi Niino (MYNN 2.5)	MM5 similarity
Long wave radiation	RRTM scheme	Asymmetric convection model 2 (ACM2)	MM5 similarity
Short wave radiation	Dudhia	Bougeault-Lacarrere scheme (BouLac)	MM5 similarity
Surface physics	Noah Land Surface Model	University of Washington	MM5 similarity
Cumulus	Kaim-Fritsch	Mellor-Yamada-Janjic (MYJ)	Eta similarity

Overall, 7 different boundary layer schemes (YSU, MYJ, MYNN2.5, ACM2, BouLac, UW and SHIN) were used for simulations. In MYJ scheme, surface scheme of Eta similarity was used while MM5 surface layer scheme was employed in the next six cases. The results of SHIN and YSU were very similar to each other; hence the results obtained by SHIN were neglected. Each model run was labeled by abbreviations in the following order: YSU, MYJ, MYN, ACM, BO, and UW.

Using temporal and spatial distribution of PM_{10}, the vertical and horizontal distribution of dust, PBL height, 10-m wind speed and wind profile were investigated. To validate the model estimations, the horizontal visibility reports of the station (Ahvaz) and hourly PM_{10} concentration (Ahvaz environmental organization) were collected. As PM_{10} data of Ahvaz city were accessible, different features of this station will be discussed further.

As PM_{10} is not directly calculated in simple running of WRF_Chem, the following equation was used [46]:

$$PM_{10}=dust\_1+dust\_2+dust\_3+0.87*dust\_4 \quad (1)$$

Results and discussion

Synoptic structure of dust

Synoptic structure and wind field were used for better understanding the atmospheric condition. At 12UTC of March 13، a low pressure was located on the Mediterranean Sea and south Europe with trough at 500 hPa (Fig. 3a). Moreover, the presence of 925 hPa through activated the Red sea low-pressure, which extended to the Saudi Arabia. The Southeast winds and pressure trough can be observed in north of Saudi Arabia and southwest of Iran (Fig. 3a) which were formed by increase of the pressure gradient between Red sea low-pressure and 1015-hPa high-pressure on the Persian Gulf. Southeast winds with the speed of 18 m/s were formed in the 925 hPa in the south west of Iran. Upward vertical motion located in west of maximum wind covers the north east of Saudi Arabia, Kuwait, southeast of Iraq and southwest of Iran. Ahvaz, Shadgan and Abadan are located in the left side of the low jet and in the upward speed part, activation of the Red Sea low-pressure along with the 500 hPa through resulted in formation of the southeast winds and upward wind speeds in Khuzestan. The mentioned processes increased the 10-m wind speed up to 13 m/s (Fig. 5) and entered the dust from the surroundings. Therefore, the condition was provided for formation of a mesoscale dust in this province. At 06UTC of March 14, the centers of 1010 hPa low-pressure in south of Iraq and 1020 hPa high pressure in south of Iran were intensified (Fig. 4a) which resulted in increase of pressure gradient and continue of the south-directed winds in the region. At the level of 925 hPa, maximum wind speed was 18 m/s directed to south-east and the upward vertical speed was observed between Abadan, Ahvaz and Shadgan (Fig. 4b).

Above conditions lead to the persistence of dust event in the region. It also increased the 10-m wind speed up to 13 m/s (Fig. 5) at 09UTC of March 14th. Reporting the code 07 indicated the local dust and horizontal visibility of 1000 m reflected its intensity. On March 14th, from 00 to 12UTC, a mesoscale dust was formed in some cities of Khuzestan province. One of the major factors in formation of mesoscale dust is the 10-m wind velocity. On March 13 and 14, form 03 to 09UTC, the 10-m wind speed increased from 10 m/s to 13 m/s (Fig. 5). From 06 to 18UTC, the code of 07 was reported; severe increase in the wind speed along with the code of 07 confirmed the internal dust.

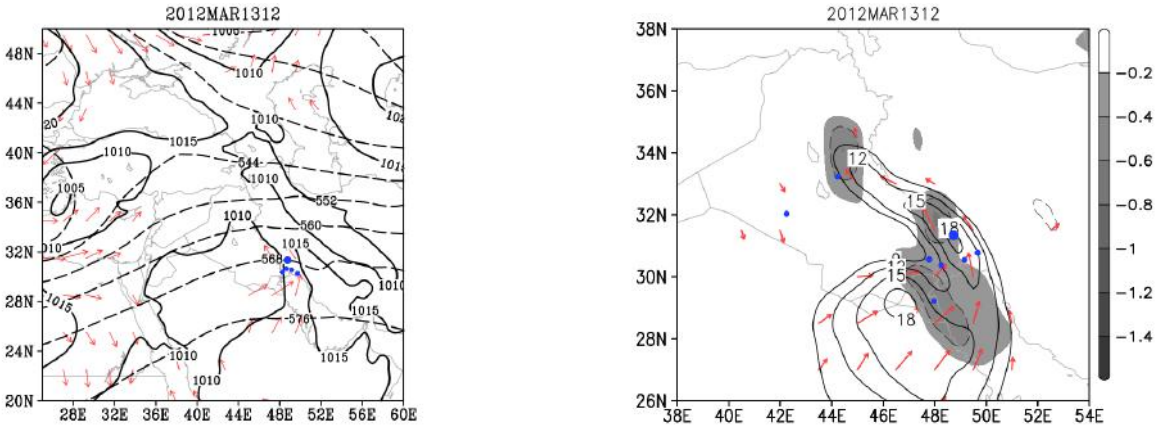

Fig. 3. a) Mean sea level pressure (solid black lines), geopotential height at 500 hPa (dashed lines) and wind direction at 925 hPa (vectors), b) wind speed (solid black lines), wind direction (red vectors) and vertical velocity (contours) on March 13

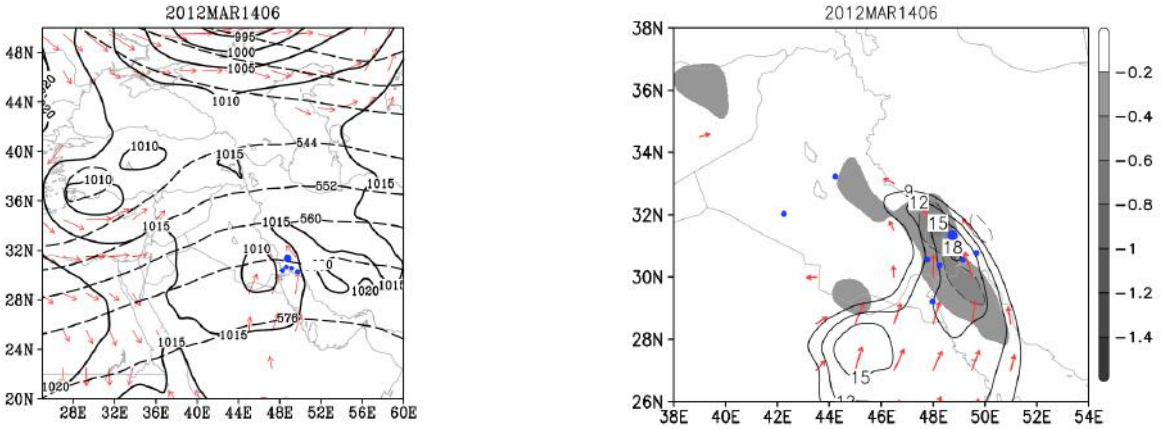

Fig. 4. a) Mean sea level pressure (solid black lines), geopotential height at 500 hPa (dashed lines) and wind direction at 925 hPa (vectors), b) wind speed (solid black lines), wind direction (red vectors) and vertical velocity (contours) on March 13

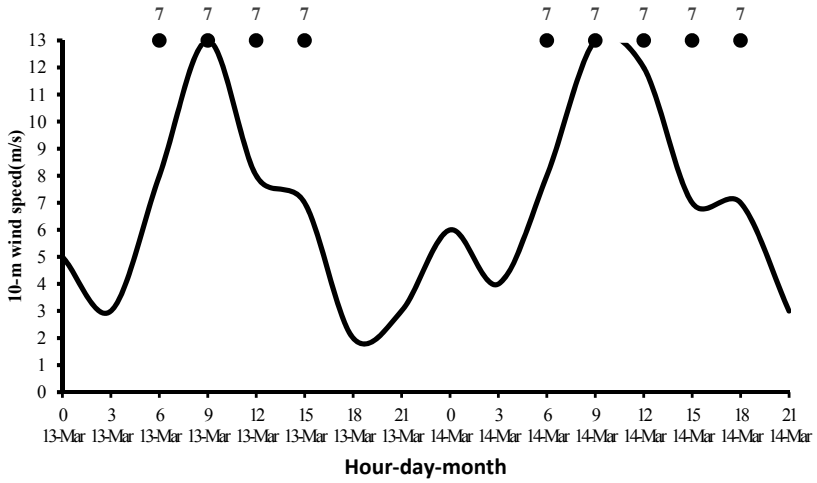

Fig. 5. The time series of observation 10-m wind speed (m/s) on March 13-14, 2012 at Ahvaz and the meteorology Phenomena

Model verification

10-m wind speed

Due to its high significance in formation of mesoscale dust, first 10-m wind speed was analyzed. On March 13 and 14, the 10-m wind speed estimated by MYN, MYJ and UW schemes showed correlation with observational data with correlation coefficients of 0.83, 0.82 and 0.76, respectively. Their correlation with ERA_I data was 0.86, 0.89 and 0.87, with the same order (Table 2). The 10-m wind speed estimated by the mentioned schemes exhibited a good correlation with the observed wind speed and primary ERA_I data (Table 2). BO scheme possessed the least correlation with the observation (0.52) and ERA_I (0.62) data (Table 2).

The correlation with the observed 10-m wind speed and ERA_I data was investigated and correlation coefficient of 0.89 was obtained which indicates their proper relationship (Table 2). Their difference however should be included in other analyses on ERA_I data.

The day-night variations of 10-m wind speed obtained from observation, ERA_I and various PBL schemes were investigated on March 14th. The maximum observed 10-m wind speed was reported 13 m/s (Table 3). The wind speed obtained by MYJ scheme (13.27 m/s) was the closer to the observed and YSU with 10.11 farther than it (Table). The minimum observed wind speed was 3 m/s while 6.52 and 4.88 m/s estimated by MYN and YSU thus YSU closer to the observation (Table 3).

Regarding the reported code of 07 which indicates local condition in occurrence or increased intensity of dust, it seems that 10 m/s variation in the wind speed within 6 h (03 to 09UTC) can provide the suitable condition for dust formation (Fig. 5).

The highest variation range of 10-m wind speed was estimated by MYJ and MYN schemes (6.75 and 5.95, respectively); both of them are smaller than the observation data 4.95 (Table 3).

10-m wind speed showed good correlation with the ERA_I data but its day-night variation range is different, this variation was 4.95 m/s for ERA_I data which was far smaller than the observational data (Table 3). It seems that ERA_I failed to indicate severe changes in 10-m wind speed.

Compared to other schemes, MYJ scheme showed significantly higher 10-m wind speed although its maximum was closer to the observed one (Table 3). Other schemes estimated similar results during the day. But their difference was higher during night; the highest wind speed was estimated by MYJ and BO while the lowest one was obtained by MYN. As the dust source was internal region and its occurrence time was between 00

Table 2. 10 m wind speed correlation coefficient with model outputs and ERA_I data

	ACM	BO	MNN	MYJ	UW	YSU
cor-mo-ob	0.73	0.52	0.83	0.82	0.76	0.74
cor-mo-era	0.83	0.62	0.86	0.89	0.87	0.83

Table 3. The maximum and minimum of 10-m wind speed on March 14

	ACM	BOU	MNN	MYJ	UW	YSU	observe	ERA_I
Max	9.66	10.71	10.15	13.27	10.51	10.11	13.00	11.87
Min	5.15	6.28	4.20	6.52	4.72	4.88	3.00	6.92
Range	4.51	4.43	5.95	6.75	5.79	5.23	10.00	4.95

to 12UTC March 14, estimation of wind speed during night has higher importance. It seems that the highest difference in estimation of 10-m wind speed can be detected in night hours. Among all of the schemes, MYN estimated wind speed better and it determined the highest increase in wind speed from 00 to 12UTC (5.95 m/s).

Day-night variation trend of 10-m wind speed in MYN and MYJ was similar to Fig. 6). Based on Table 3, they had the highest correlation with the observational data. MYJ estimated the maximum wind speed at 09UTC in accordance with the observation, but the minimum of wind speed at night showed a huge error Fig. 6). Therefore, among the six PBL schemes, MYJ seems to be a proper choice for estimating the magnitude and variation range during day time as well as MYN for the minimum wind speed at night.

On March 14th, two series of observation data and ERA_I showed a difference during night hours. They however showed a good consistency in the mid-day hours (12UTC) (Fig. 6). Therefore, ERA_I data, which were used for simulation had some differences (especially in night hours) in terms of value and trend of variation with the observations; in such a way that they showed the minimum wind speed higher than the observations.

PM_{10}

Dust events will make the atmosphere turbidity and hence they can reduce the horizontal visibility. Horizontal visibility decreases if the dust concentration increases, so the horizontal visibility means more severe dust. On March 13 and 14, the correlation between the observed horizontal visibility and PM_{10} was -0.89 (Table 4) indicating their inverse relationship. Increase of PM_{10} resulted in reduction of the horizontal visibility. As reduced horizontal visibility could be also due to air pollution, fog or cloudy condition, the variation in these two could be not consistent. Regarding the satellite images on March 14th, Ahvaz was cloudy on that day and it should be considered as another reason for the reduced visibility.

PM_{10} obtained by the model (MYN and UW) showed correlation with the measured values by 0.67 and 0.63, respectively. Their correlation with the horizontal visibility was -0.76 and -0.73, respectively (Table 4). The lowest correlation between the PM_{10} model-estimated values and observation was determined for BO scheme (0.37).

During the two days, all six schemes have overestimated the PM_{10} concentration (Table 5). On March 14, maximum observed PM_{10} was 646 µg/m^3 which declined the visibility to 1000 m. ACM and BO schemes estimated maximum PM_{10} as

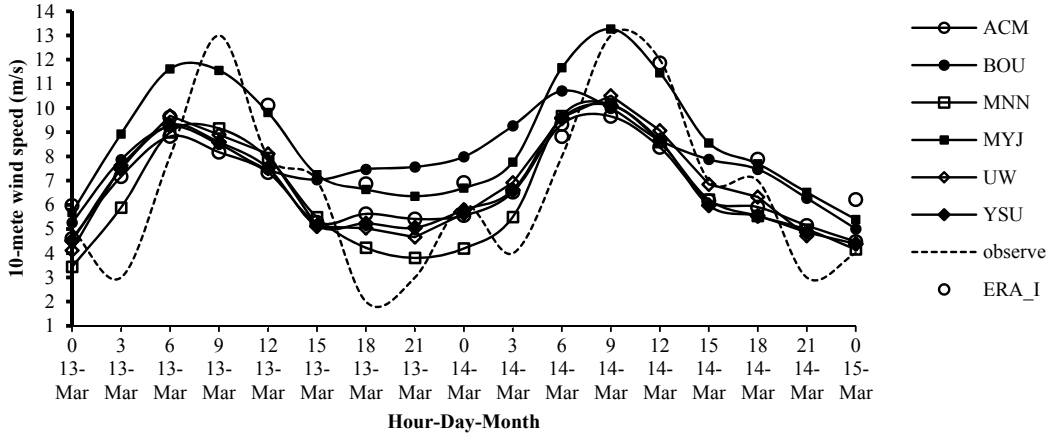

Fig. 6. The time series of 10 m wind speed (m/s) from six simulations, observation and ERA_I on March 13-14, 2012

Table 4. Correlation coefficient PM_{10} of model output, observation PM_{10} and observation visibility

	ACM	BO	MNN	MYJ	UW	YSU
Model-PM_{10} Observ-PM_{10}	0.50	0.37	0.67	0.55	0.63	0.51
Model visibility	-0.64	-0.55	-0.76	-0.72	-0.73	-0.69

Table 5. Maximum, minimum and variation range of model PM_{10} µg/m^3

	ACM	BO	MNN	MYJ	UW	YSU	PM_{10}	Vis
Max	2134	2474	2530	5081	2794	2659	646	7000
Min	768	1472	429	1937	658	1015	146	1000
D	1366	1001	2101	3145	2136	1644	501	6000

2134 and 2474 µg/m^3 respectively (Table 5). Other schemes estimated even higher PM_{10} values, the lowest observed PM_{10} was also 146 µg/m^3 which decreased the horizontal visibility to 7000 m. MYN and UW schemes estimated the lowest minimum PM_{10} values (429 and 658 µg/m^3 respectively) (Table 5). High difference in PM_{10} estimation compared to the observed values was also mentioned in the previous studies [27, 33, 42].

Maximum PM_{10} estimated by MYJ schemes (5081 µg/m^3) showed a significant difference with the other schemes (Table 5). 10-m wind speed (13.27 m/s) and PM_{10} concentration (5081 µg/m^3) estimated by this scheme exhibited a significant difference with other schemes.

Day-night variation diagram of PM_{10} showed that BO, MYN, UW and YSU schemes were relatively similar with identical fluctuations (Fig. 7). MYN estimated lower values in night hours in line with the fact that it estimated the lowest night wind speed among all the studied schemes. The role of 10-m wind speed is evident in formation of dust events. Therefore, the schemes with better estimation of 10-m wind speed will had better performance in estimating the PM_{10} concentration. The variation in 10-m wind speed from 00 to 12UTC is of crucial importance in local dust emission.

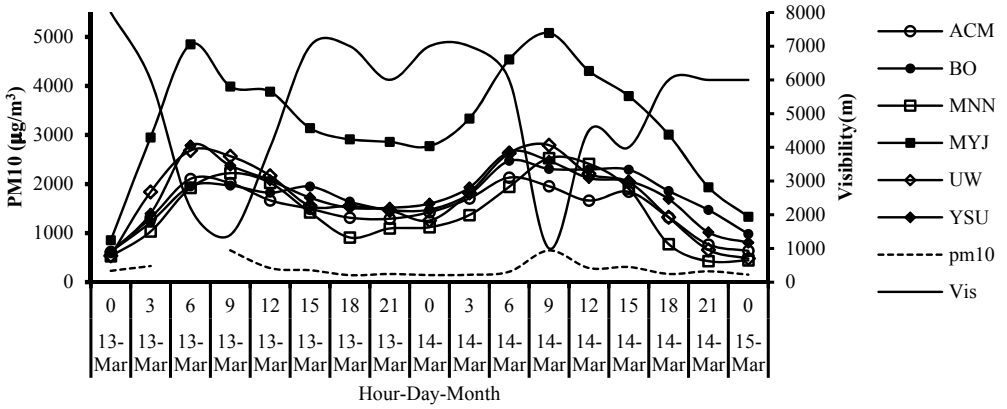

Fig. 7. The time series of PM_{10} from observation and six simulations µg/m^3, visibility on March 13-14, 2012

Comparison boundary layer height, wind speed and PM_{10}

There is no observation data for comparing the height of boundary layer, hence primary ERA_I data were used as observation. On March 14, except for MYJ, the estimated PBL height of the schemes were lower than the ERA_I (Fig. 8). The PBL height obtained by these 5 schemes during day hours showed more consistency with each other and ranged from 700 to 900 m. Their difference however increased during night hours with different variation trends. Regarding different physical mechanisms used in these schemes for day hours with static stability of lower levels of the atmosphere, the models will perform differently. The obtained results were similar to the other studies [36, 24, 27].

Compared with other schemes, the PBL height obtained by MYJ showed a significant difference and was higher than others (Fig. 8). This difference can be seen in both the value of PBL height and its temporal variation. It got close to the other schemes in 12UTC of March 14. This could be due to the effect of dust in the previous hours. Presence of dust affected the temperature and wind in higher layers of the atmosphere and the growth of PBL was lower than the March 13. The differences in the value and variation trend of 10-m wind speed, PBL height and PM_{10} were higher in case of MYJ scheme when compared with others.

In other studies [43], regarding the calculation structure (local) of MYJ scheme, it is anticipated that its PBL height estimation to be lower than those of YSU and MYJ local schemes. Nevertheless, as the surface schemes used in MYJ is different from other schemes, the role of surface condition on PBL height simulation cannot be denied.

Vertical growth and extension of the boundary layer is accompanied with variations in wind speed and formation of turbulence in the atmosphere. Mesoscale variation of wind is effective in rise of dust and its transfer to the boundary layer (Marsham 2008).

In continue the wind speed and PM_{10} concentration in higher layers will be discussed. For this section, there was no observation data; hence, the model outputs were compared with ERA_I data. At 975 hPa level, all the schemes estimated higher wind speed (compared to ERA_I data) (Fig. 9). Their variation trends completely coincided from 9 to 12UTC (mid-day); but they were different for night hours. This difference increased at 06UTC. The model-estimated PM_{10} concentration of the same level at 9UTC of March 14

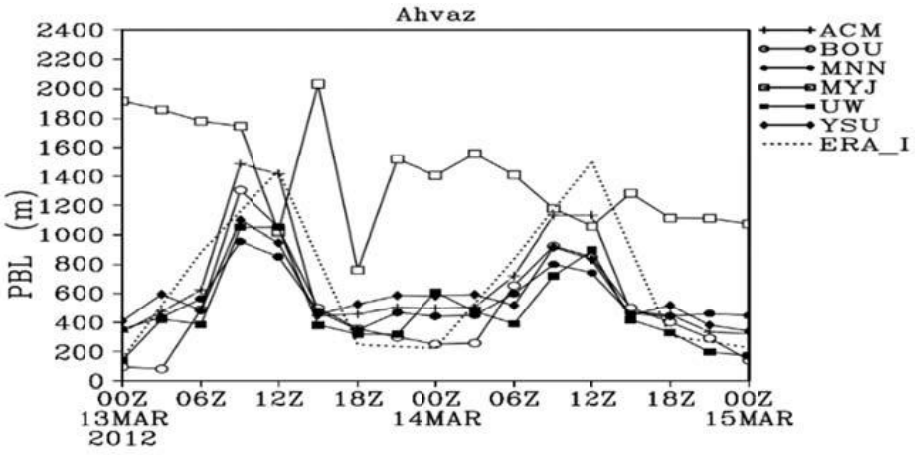

Fig. 8. The time series of PBL height (m) from six simulations, on March 13-14, 2012

showed a maximum value which is consistent with the maximum measured surface PM_{10}. MYJ and ACM schemes estimated the highest and lowest concentrations, respectively (Fig. 9). Increase of wind speed resulted in increase of PM_{10} with a delay. In such a way that increase of wind speed at 03UTC resulted in increase of PM_{10} at 09 and 12UTC. Regarding lower extension of the PBL in mid-day hours of March 14, compared to March 13 as well as reduced wind speed and increase of PM_{10}, it seems that the reduction of boundary layer height along with less turbulence resulted in enhanced PM_{10} concentration. The results are in accompanied with the theoretical discussion and other studies. During night hours, the estimated concentrations of all the schemes were relatively similar but BO showed a small difference. Although this scheme had the wind speed with higher consistency with ERA_I, but it had huge error in estimation of PM_{10} during night hours.

Vertical extension of dust

Temporal variation and vertical extension of dust were similar in all six schemes up to the level of 850 hPa and showed the increase of dust concentration near the surface from 06 to 12UTC of March 14 (Fig. 10). As the dust event was internal on March 14 and the environment condition had influences on its occurrence, it was mostly focused on 900-hPa level with limited vertical extension. Similar to the previous results, MYJ estimated the highest concentration compared to the other schemes (Fig. 10).

For all the schemes, the maximum wind speed was formed between 00 and 06UTC (low-level jet) (Fig. 10). The maximum magnitude and the time of occurrence were however different for different schemes. In MYN and UW schemes, maximum wind speed (24 m/s) occurred at 03UTC (Fig. A and B). In other schemes, the maximum wind speed reached to 20 m/s. the mentioned two schemes showed more consistency with the observation according to the previous discussions on 10-m wind speed and surface PM_{10}. Comparison of the wind fields and the previous results indicated that these two schemes are more suitable for estimation of mesoscale dust in Ahvaz.

From 15 to 18UTC of the same day and in the level of 900 hPa, an increase can be seen in the dust concentration (Fig. 10) which is in line with the increase in the wind speed in the previous hours (03 to 09UTC). This means that as the result of the increase in the wind speed in the low levels of the atmosphere from 03 to 09UTC, the

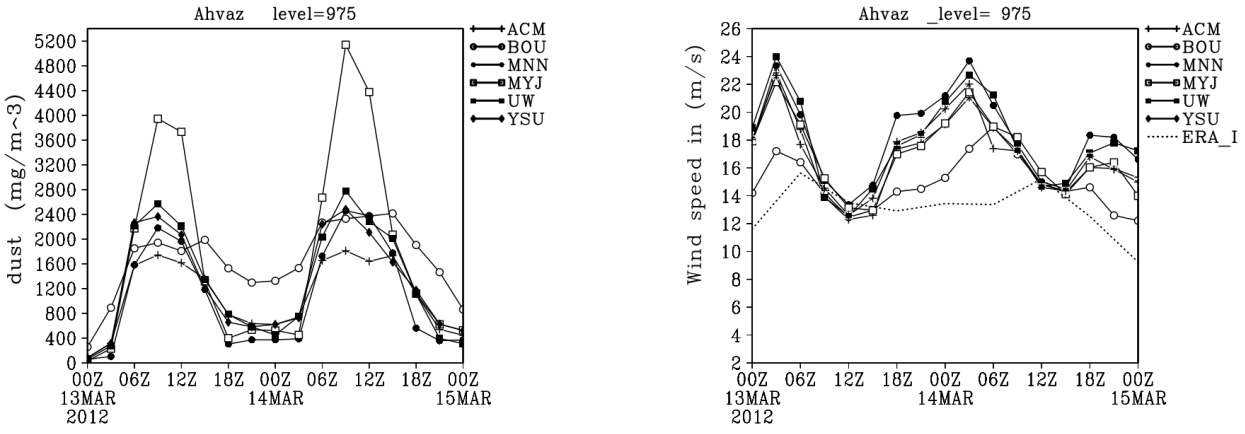

a b

Fig. 9. The time series of a) PM10 µg/m3 , b) wind speed (m/s) at 975hPa on March 13-14, 2012

10-m wind speed was enhanced and gave rise of dust in the region. After the decline in the wind speed at the level of 975-900 hPa at 12UTC (midday hour) the dust particles were trapped beneath this level and increased the dust concentration in that layer.

Conclusion

WRF_Chem model was implemented to simulate the mesoscale dust event in Khuzestan province (Ahvaz station) on March 13 and 14. The model was run with six different schemes. The results indicated that among all the boundary layer schemes, the variation trend estimated by MYN scheme is more consistent with the observed PM_{10} values. Due to the highest correlation of the 10-m wind speed, horizontal visibility, PM_{10} respectively with 0.83, -0.76 and 0.76 values and the highest consistency with the day-night variation of PM_{10}, MYN scheme can be selected as the most suitable scheme. UW scheme will be placed in the second rank.

Variation of 10-m wind speed from 00 to 12UTC plays a major role in emission of local dust. Therefore, schemes with better estimation of 10-m wind speed and night wind speed will perform better in estimation of PM_{10} and dust concentration.

Although the results of MYJ scheme showed correlation with observed horizontal visibility and PM_{10} with consistent temporal variation, but as it determined PM_{10} concentration with high difference, it cannot be considered as a suitable scheme. Regarding the different surface scheme used in MYJ scheme, this scheme showed a significant difference with other schemes indicating the significant role of surface schemes in determination of the fluxes used in the PBL. Moreover, regarding the correlation coefficients of the observed data and the model output as well as the variation trend, BO was determined as the most improper scheme.

Increase of wind speed in 950 hPa level has an effective role in the development of local dust. The two schemes of MYN and UW estimated the maximum wind speed along the low level jet axis in 03UTC as 24 m/s.

The dust concentration from 00 to 12UTC showed the highest consistency with observed PM_{10} and horizontal visibility.

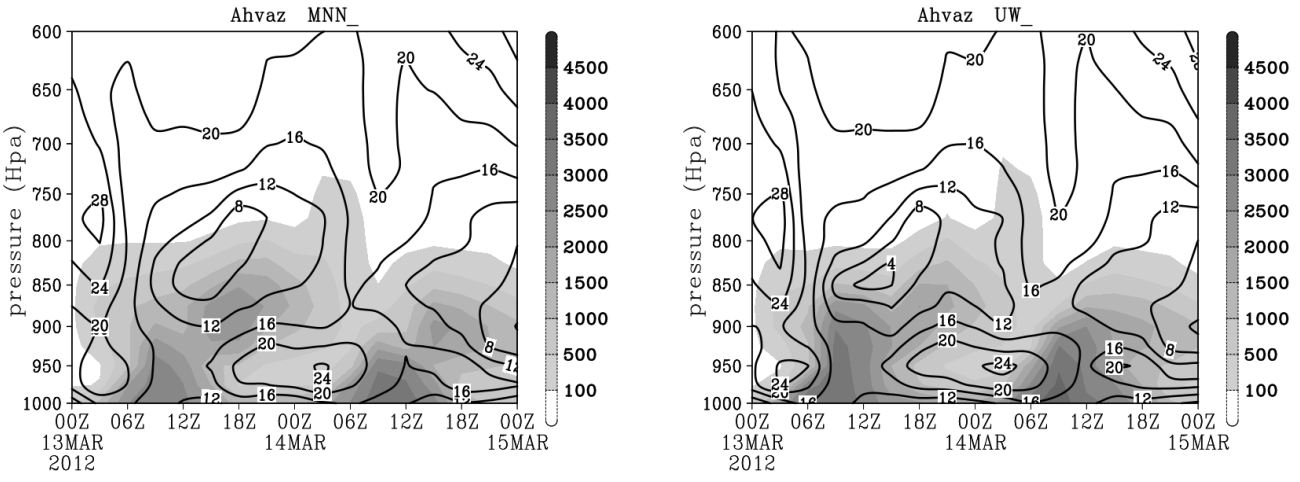

a b

Fig. 10. The time series of wind speed (m/s) and dust concentration μg/m^3 for a) MNN, B) UW schemes on March 13-14, 2012

In the case of mesoscale dust occurred in March 13 and 14 in Khuzestan province, using WRF-Chem model, the results showed that the model was not have to predict/simulate the PM_{10} concentration. The difference between model outputs and observation could be due to the initial and boundary condition. In addition, the dust scheme that were used in this model was GOCART which can be substituted with other schemes in the future studies.

Financial supports

Islamic Azad University of Ahvaz has been the financial supporter of this article.

Competing interests

The authors from various organizations including Azad university branch Ahvaz and Science and research also Atmospheric Science & Meteorological Research Center (ASMERC) have contributed to this article.

Acknowledgements

We are grateful to the Atmospheric Science & Meteorological Research Center (ASMERC) Chief and Executive Officer that in the preparation of the article, they provided the necessary conditions and had a good cooperation

Ethical considerations

It is also an original article and has not previously been published by any other publication.

References

1. Heydarian P, Azhdari A, Juddake M, Khatooni JD, Shahbazi R. Identification of Internal Origin of Dust storm Using Remote Sensing, GIS and Geology (Case Study: Khouzestan). Journal of Earth Sciences.2017 Autum, 27(105):33-46. [in Persian].
2. Marsham JH, Parker DJ, Grams CM, Johnson BT, Grey WM, Ross AN. Observations of mesoscale and boundary-layer scale circulations affecting dust transport and uplift over the Sahara. Atmospheric Chemistry and Physics. 2008;8(23):6979-93.
3. Cavazos-Guerra C, Todd MC. Model simulations of complex dust emissions over the Sahara during the West African monsoon onset. Advances in Meteorology. 2012;2012.
4. Engelstaedter S, Tegen I, Washington R. North African dust emissions and transport. Earth-Science Reviews. 2006 Nov 1;79(1-2):73-100.
5. Chaboureau JP, Tulet P, Mari C. Diurnal cycle of dust and cirrus over West Africa as seen from Meteosat Second Generation satellite and a regional forecast model. Geophysical research letters. 2007 Jan;34(2).
6. Warner TT, Sheu RS. Multiscale local forcing of the Arabian Desert daytime boundary layer, and implications for the dispersion of surface-released contaminants. Journal of Applied Meteorology. 2000 May;39(5):686-707.
7. Chen F, Dudhia J. Coupling an advanced land surface–hydrology model with the Penn State–NCAR MM5 modeling system. Part I: Model implementation and sensitivity. Monthly Weather Review. 2001 Apr;129(4):569-85.
8. Chen S, Huang J, Zhao C, Qian Y, Leung LR, Yang B. Modeling the transport and radiative forcing of Taklimakan dust over the Tibetan Plateau: A case study in the summer of 2006. Journal of Geophysical Research: Atmospheres. 2013 Jan 16;118(2):797-812.
9. Lu H, Shao Y. A new model for dust emission by saltation bombardment. Journal of Geophysical Research: Atmospheres. 1999 Jul 27;104(D14):16827-42.
10. Tegen I. Modeling the mineral dust aerosol cycle in the climate system. Quaternary Science Reviews. 2003 Sep 1;22(18-19):1821-34.
11. Shao Y, Ishizuka M, Mikami M, Leys JF. Parameterization of size-resolved dust emission and validation with measurements. Journal of Geophysical Research: Atmospheres. 2011 Apr 27;116(D8).
12. Allen CJ, Washington R. The low-level jet dust emission mechanism in the central Sahara: Observations from Bordj-Badji Mokhtar during the June 2011 Fennec Intensive Observation Period. Journal of Geophysical Research: Atmospheres. 2014 Mar 27;119(6):2990-3015.
13. Marticorena B, Bergametti G. Modeling the atmospheric dust cycle: 1. Design of a soil-derived dust emission scheme. Journal of Geophysical Research: Atmospheres. 1995 Aug 20;100(D8):16415-30.
14. Pokharel A, Kaplan M. Dust Climatology of the NASA Dryden Flight Research Center (DFRC) in Lancaster, California, USA. Climate. 2017 Mar;5(1):15.
15. Washington R, Todd MC. Atmospheric controls on mineral dust emission from the Bodélé Depression, Chad: The role of the low level jet. Geophysical Research Letters. 2005 Sep;32(17).
16. Daum PH, Kleinman LI, Springston SR, Nunnermacker LJ, Lee YN, Weinstein-Lloyd J, Zheng J, Berkowitz CM. A comparative study of O3 formation in the Hous-

ton urban and industrial plumes during the 2000 Texas Air Quality Study. Journal of Geophysical Research: Atmospheres. 2003 Dec 16;108(D23).
17. Banta RM, Senff CJ, Nielsen-Gammon J, Darby LS, Ryerson TB, Alvarez RJ, Sandberg SP, Williams EJ, Trainer M. A bad air day in Houston. Bulletin of the American Meteorological Society. 2005 May;86(5):657-70.
18. Zhang F, Bei N, Nielsen-Gammon JW, Li G, Zhang R, Stuart A, Aksoy A. Impacts of meteorological uncertainties on ozone pollution predictability estimated through meteorological and photochemical ensemble forecasts. Journal of Geophysical Research: Atmospheres. 2007 Feb 27;112(D4).
19. Storm B, Basu S. The WRF model forecast-derived low-level wind shear climatology over the United States Great Plains. Energies. 2010;3(2):258-76.
20. Carvalho D, Rocha A, Gómez-Gesteira M, Santos C. A sensitivity study of the WRF model in wind simulation for an area of high wind energy. Environmental Modelling & Software. 2012 Jul 1;33:23-34.
21. Bao JW, Michelson SA, Persson PO, Djalalova IV, Wilczak JM. Observed and WRF-simulated low-level winds in a high-ozone episode during the Central California Ozone Study. Journal of Applied Meteorology and Climatology. 2008 Sep;47(9):2372-94.
22. Cheng FY, Chin SC, Liu TH. The role of boundary layer schemes in meteorological and air quality simulations of the Taiwan area. Atmospheric environment. 2012 Jul 1;54:714-27.
23. Gilliam RC, Godowitch JM, Rao ST. Improving the horizontal transport in the lower troposphere with four dimensional data assimilation. Atmospheric environment. 2012 Jun 1;53:186-201.
24. Hu XM, Doughty DC, Sanchez KJ, Joseph E, Fuentes JD. Ozone variability in the atmospheric boundary layer in Maryland and its implications for vertical transport model. Atmospheric Environment. 2012 Jan 1;46:354-64
25. Storm B, Dudhia J, Basu S, Swift A, Giammanco I. Evaluation of the weather research and forecasting model on forecasting low-level jets: Implications for wind energy. Wind Energy: An International Journal for Progress and Applications in Wind Power Conversion Technology. 2009 Jan;12(1):81-90.
26. García-Díez M, Fernández J, Fita L, Yagüe C. Seasonal dependence of WRF model biases and sensitivity to PBL schemes over Europe. Quarterly Journal of the Royal Meteorological Society. 2013 Jan 1;139(671):501-14.
27. Bossioli E, Tombrou M, Dandou A, Athanasopoulou E, Varotsos KV. The role of planetary boundary-layer parameterizations in the air quality of an urban area with complex topography. Boundary-layer meteorology. 2009 Apr 1;131(1):53-72.
28. Hu XM, Nielsen-Gammon JW, Zhang F. Evaluation of three planetary boundary layer schemes in the WRF model. Journal of Applied Meteorology and Climatology. 2010 Sep;49(9):1831-44.
29. Troen IB, Mahrt L. A simple model of the atmospheric boundary layer; sensitivity to surface evaporation. Boundary-Layer Meteorology. 1986 Oct 1;37(1-2):129-48.
30. Stull RB. Mean boundary layer characteristics. InAn Introduction to Boundary Layer Meteorology 1988 (pp. 1-27). Springer, Dordrecht.
31. Stensrud DJ. Parameterization schemes: keys to understanding numerical weather prediction models. Cambridge University Press; 2009 Dec 3.
32. Stull RB. Static stability—An update. Bulletin of the American Meteorological Society. 1991 Oct;72(10):1521-30.
33. Misenis C, Hu XM, Krishnan S, Zhang Y, Fast J. Sensitivity of WRF/Chem predictions to meteorological schemes. In86th Annual Conference/14th Joint Conference on the Applications of Air Pollution Meteorology with the A&WMA, Atlanta, GA, USA 2006 Jan (Vol. 27).
34. Xie B, Fung JC, Chan A, Lau A. Evaluation of nonlocal and local planetary boundary layer schemes in the WRF model. Journal of Geophysical Research: Atmospheres. 2012 Jun 27;117(D12).
35. Alapaty K, Raman S, Niyogi DS. Uncertainty in the specification of surface characteristics: A study of prediction errors in the boundary layer. Boundary-Layer Meteorology. 1997 Mar 1;82(3):475-502.
36. Banks RF, Tiana-Alsina J, Baldasano JM, Rocadenbosch F, Papayannis A, Solomos S, Tzanis CG. Sensitivity of boundary-layer variables to PBL schemes in the WRF model based on surface meteorological observations, lidar, and radiosondes during the HygrA-CD campaign. Atmospheric Research. 2016 Jul 1;176:185-201.
37. Hu XM, Klein PM, Xue M. Evaluation of the updated YSU planetary boundary layer scheme within WRF for wind resource and air quality assessments. Journal of Geophysical Research: Atmospheres. 2013 Sep 27;118(18):10-490.
38. Jankov I, Gallus Jr WA, Segal M, Shaw B, Koch SE. The impact of different WRF model physical parameterizations and their interactions on warm season MCS rainfall. Weather and forecasting. 2005 Dec;20(6):1048-60.
39. Jankov I, Schultz PJ, Anderson CJ, Koch SE. The impact of different physical parameterizations and their interactions on cold season QPF in the American River basin. Journal of Hydrometeorology. 2007 Oct;8(5):1141-51.
40. Li X, Pu Z. Sensitivity of numerical simulation of early rapid intensification of Hurricane Emily (2005) to cloud microphysical and planetary boundary layer parameterizations. Monthly Weather Review. 2008 Dec;136(12):4819-38.
41. Gan CM, Wu Y, Madhavan BL, Gross B, Moshary F. Application of active optical sensors to probe the vertical structure of the urban boundary layer and assess anomalies in air quality model PM2.5 forecasts. Atmo-

spheric environment. 2011 Dec 1;45(37):6613-21.
42. Zhang Y, Bocquet M, Mallet V, Seigneur C, Baklanov A. Real-time air quality forecasting, part I: History, techniques, and current status. Atmospheric Environment. 2012 Dec 1;60:632-55.
43. Misenis C, Zhang Y. An examination of sensitivity of WRF/Chem predictions to physical parameterizations, horizontal grid spacing, and nesting options. Atmospheric Research. 2010 Aug 1;97(3):315-34.
44. Werner M, Kryza M, Ojrzynska H, Skjoth CA, Walaszek K, Dore AJ. Application of WRF-Chem to forecasting PM10 concentration over Poland. International Journal of Environment and Pollution. 2015;58(4):280-92.
45. Rizza U, Barnaba F, Miglietta MM, Mangia C, Di Liberto L, Dionisi D, Costabile F, Grasso F, Gobbi GP. WRF-Chem model simulations of a dust outbreak over the central Mediterranean and comparison with multisensor desert dust observations. Atmospheric Chemistry and Physics. 2017;17(1):93.
46. WRF-Chem Tutorial, Feb. 6, 2017